Inorganic Chemistry

ARTICLE

pubs.acs.org/IC

Suppression of Magnetic Order in $Sr_3Fe_2O_4Cl_2$ by Fe-Site Substitution by Cobalt

Edward Dixon and Michael A. Hayward*

Inorganic Chemistry Laboratory, Department of Chemistry, University of Oxford, South Parks Road, Oxford OX1 3QR, United Kingdom

Supporting Information

ABSTRACT: The low-temperature topotactic reduction of $Sr_3Fe_{2-x}Co_xO_5Cl_2$ oxychloride phases with LiH allows the preparation of phases of composition $Sr_3Fe_{2-x}Co_xO_4Cl_2$ ($0 \leq x \leq 1$). The reduced phases adopt body-centered tetragonal structures which are isostructural with $Sr_3Fe_2O_4Cl_2$ and contain square-planar $(Fe/Co)O_4$ centers connected into apex-linked sheets, analogous to the CuO_2 sheets present in superconducting cuprate phases. As the cobalt concentration in $Sr_3Fe_{2-x}Co_xO_4Cl_2$ is increased the antiferromagnetic order of the $Sr_3Fe_2O_4Cl_2$ host phase is suppressed, ultimately leading to spin-glass behavior, at low temperature, in $Sr_3Fe_{2-x}Co_xO_4Cl_2$ phases with $x \geq 0.8$. The limited influence of cobalt substitution on the reactions which form the $Sr_3Fe_{2-x}Co_xO_4Cl_2$ phases is discussed and contrasted to that of the related $SrFeO_{3-\delta}$−$SrFeO_2$ system.

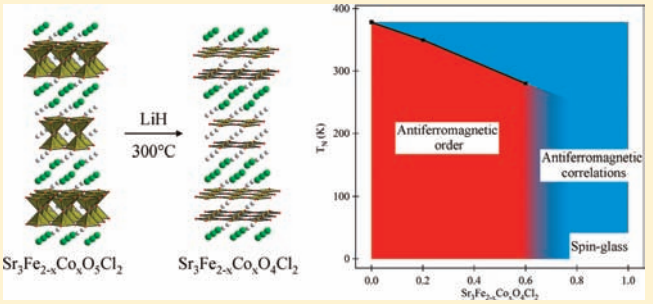

INTRODUCTION

Since the discovery of high-temperature superconductivity in complex copper oxides, there has been great interest in preparing materials which contain square-planar MO_4 transition-metal centers, particularly when these centers are arranged into corner-linked sheets, analogous to the CuO_2 sheets present in the superconducting cuprate phases. However despite extensive investigations, very few thermodynamically stable phases have been discovered which exhibit this structural motif in the absence of copper.

Given the apparent low thermodynamic stability of extended oxide phases containing square-planar transition metal centers, a logical synthetic approach is to exploit kinetically controlled chemical processes to prepare suitable metastable phases. Topotactic reduction reactions, which exploit the large difference between cation and anion mobilities in complex oxides to deintercalate oxide ions from extended solids, facilitate the preparation of kinetically stabilized phases which contain extended arrays of transition-metal centers in unusual coordination environments and oxidation states. This includes phases which contain apex-linked sheets of planar MO_4 centers. Thus, for example, the reduction of the Ni(III) oxides $LaNiO_3$ and $LaSrNiO_4$ at low-temperature yields the Ni(I) phases $LaNiO_2$ and $LaSrNiO_3$, respectively,[1,2] which contain extended arrays of corner-linked Ni^IO_4 square-planes. Specifically $LaNiO_2$ forms the so-called infinite-layer structure and is isostructural with $Ca_{0.84}Sr_{0.16}CuO_2$[3] while $LaSrNiO_3$ adopts a one-dimensional structure isostructural with Sr_2CuO_3[4] as shown in Figure 1.

The formation of anion deficient phases such as $LaNiO_2$ and $LaSrNiO_3$, which contain Ni(I) centers in square-planar coordination sites, is attributable to the favorable crystal-field stabilization energy associated with the d^9 electron count of these ions in such a coordination environment. It is however possible to prepare phases with extended sheets of corner-linked MO_4 centers in the absence of such favorable interactions, as demonstrated by the reduction of $SrFeO_3$ and $Sr_3Fe_2O_6$ to the respective Fe(II) phases $SrFeO_2$ and $Sr_3Fe_2O_5$,[5,6] both of which contain arrays of apex-linked $Fe^{II}O_4$ planar centers as shown in Figure 1.

In this instance, it is not clear what directs $SrFeO_2$ and $Sr_3Fe_2O_5$ to adopt anion deficient structures which contain Fe(II) centers in these highly unusual square-planar coordination sites. The high-spin d^6 electronic configuration adopted by the Fe(II) centers in these phases is offered no obvious stabilization by square-planar coordination geometries. Likewise the large scale rearrangement of the anion lattice during the course of the reduction reactions that lead to the formation of both $SrFeO_2$ and $Sr_3Fe_2O_5$, make it hard to rationalize the structures adopted by these phases on the basis of the coordination preferences of the Sr^{2+} A-cations, in contrast to a number of related anion deintercalation reactions.[7,8]

To shed some light on the structural selectivity exhibited during the formation of $SrFeO_2$, a recent study by Kageyama et al. investigated the effect of replacing some of the iron centers with cobalt or manganese.[9] They observed that at low levels of substitution the reduction of $SrFe_{1-x}(Mn/Co)_xO_{3-\delta}$ substrate phases led as expected to the formation of the corresponding

Received: April 21, 2011
Published: June 29, 2011

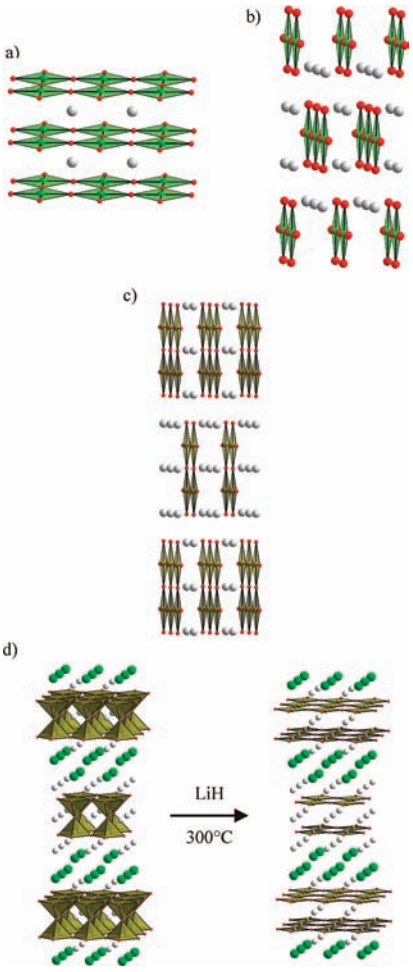

Figure 1. (a) Infinite layer structure adopted by $LaNiO_2$, $Ca_{0.84}Sr_{0.16}CuO_2$, and $SrFeO_2$. (b) The structure of $LaSrNiO_3$. (c) The structure of $Sr_3Fe_2O_5$. (d) The structural transformation which occurs during topotactic reduction of $Sr_3Fe_2O_5Cl_2$ to $Sr_3Fe_2O_4Cl_2$.

infinite layer $SrFe_{1-x}(Mn/Co)_xO_2$ phases. However, at substitution levels of greater than 30%, reduction reactions led to alternative products which are yet to be identified. The sensitivity of the reduction reactions of $SrFe_{1-x}(Mn/Co)_xO_{3-\delta}$ phases to cation substitution does suggest that the d^6 electronic configuration of the Fe(II) centers plays some role in directing the formation of anion deficient structures with square-planar $Fe^{II}O_4$ coordination sites. However, a more immediate consequence of the limited range of substituted $SrFe_{1-x}(Mn/Co)_xO_2$ phases which can be prepared is the frustration of the second goal of the Kageyama investigation: to probe the electronic behavior of substituted $SrFeO_2$ phases as a function of a wide range of d-electron count.[9]

Recently we reported the preparation of the Fe(II) phase $Sr_3Fe_2O_4Cl_2$ via the topotactic reduction of $Sr_3Fe_2O_5Cl_2$ with LiH.[10] In this instance the formation of the anion deficient structure adopted by $Sr_3Fe_2O_4Cl_2$, which also contains sheets of apex-linked planar $Fe^{II}O_4$ centers (Figure 1), can be seen to be directed by the coordination preferences of the Sr^{2+} A-cations. As a result the reactions which form $Sr_3Fe_2O_4Cl_2$ are much more tolerant to cation substitution than those which form $SrFeO_2$. Here we report the effects of cobalt substitution on the crystal structure and magnetic behavior of $Sr_3Fe_{2-x}Co_xO_4Cl_2$ phases $(0 \le x \le 1)$ to complement and contrast those of the analogous $SrFe_{1-x}Co_xO_2$ $(0 \le x \le 0.3)$ phases.

EXPERIMENTAL SECTION

Preparation of $Sr_3Fe_{2-x}Co_xO_5Cl_2$ Phases. Samples of $Sr_3Fe_{2-x}Co_xO_5Cl_2$ (x = 0.2, 0.6, 0.8, 1) were prepared by the direct-combination route previously described by Weller et al. for the synthesis of $Sr_3FeCoO_5Cl_2$.[11] Suitable quantities of SrO (prepared by the decomposition of $SrCO_3$ at 1100 °C under vacuum), $SrCl_2$ (dried at 180 °C under vacuum), Fe_2O_3 (99.99%), and $Sr_2Co_2O_5$ (prepared using the method described by Grenier et al.[12]) were thoroughly mixed using an agate pestle and mortar in an argon filled glovebox (O_2 and H_2O levels <1 ppm). The resulting mixtures were then sealed under vacuum in silica ampules and heated at 850 °C for 2 periods of 24 h with one intermediate grinding. X-ray powder diffraction data sets collected from the $Sr_3Fe_{2-x}Co_xO_5Cl_2$ samples were consistent with single phase materials with lattice parameters which span the range between the values reported for $Sr_3Fe_2O_5Cl_2$ and $Sr_3FeCoO_5Cl_2$ as detailed in the Supporting Information.[11]

Reduction of $Sr_3Fe_{2-x}Co_xO_5Cl_2$ Phases. The reduction of the $Sr_3Fe_{2-x}Co_xO_5Cl_2$ (x = 0.2, 0.6, 0.8, 1) phases was performed using LiH as a solid-state reducing agent[13] in a similar manner to that reported for the topotactic reduction reaction of $Sr_3Fe_2O_5Cl_2$.[10] Small samples (~ 300 mg) of the required $Sr_3Fe_{2-x}Co_xO_5Cl_2$ phase were ground together in a 1:4 molar ratio with LiH in an argon filled glovebox. These mixtures were then sealed under vacuum in Pyrex ampules and heated at temperatures between 210 and 400 °C to monitor the temperature dependence of the reduction reactions.

Because of the hazards associated with the production of hydrogen gas when using LiH as a reducing agent,[13] large-scale samples suitable for characterization by neutron powder diffraction were synthesized in a sealed Parr Series 4740 pressure vessel which is capable of withstanding the hydrogen gas pressures generated by these reactions. Approximately 4 g of the required $Sr_3Fe_{2-x}Co_xO_5Cl_2$ phase was mixed, in an argon filled glovebox, with 4 mol equivalents of LiH and loaded into an alumina finger which was then sealed inside the pressure vessel. The pressure vessel was then evacuated, sealed, and heated so that the sample was held at a temperature of 300 °C for 4 periods of 24 h with intermediate grinding. After reaction, samples were washed with 4 × 100 mL aliquots of methanol, under nitrogen, to remove any lithium containing phases (LiH and Li_2O) before being dried under vacuum.

Characterization. X-ray powder diffraction data were collected from samples contained within homemade gastight sample holders using a PANalytical X'Pert diffractometer incorporating an X'celerator position sensitive detector (monochromatic Cu $K_{\alpha 1}$ radiation). Neutron powder diffraction data were collected from samples contained within vanadium cans which had been sealed under argon with indium washers. Table 1 details the instruments, temperature ranges, and incident wavelengths at which data were collected. Rietveld profile refinement against these data was performed using the GSAS suite of programs.[14] Magnetization measurements were collected using a Quantum Design MPMS SQUID magnetometer. Magnetization data indicated that all the reduced samples contained small quantities of ferromagnetic elemental iron and cobalt, which masked the magnetic behavior of the bulk phases. The paramagnetic susceptibility of samples was therefore measured using a "ferromagnetic subtraction" technique described previously[15] and described fully in the Supporting Information.

RESULTS

Reactivity of $Sr_3Fe_2O_4Cl_2$. X-ray powder diffraction data collected from the products of reactions between $Sr_3Fe_{2-x}Co_xO_5Cl_2$ (x = 0.2, 0.6, 0.8, 1) phases and LiH reveal that at temperatures below 300 °C no reactions occur. Reactions performed

dx.doi.org/10.1021/ic200832n |Inorg. Chem. 2011, 50, 7250–7256

Table 1. Details of the Neutron Powder Diffraction Experiments Performed on the $Sr_3Fe_{2-x}Co_xO_4Cl_2$ Samples

	instrument in temperature range		
	5 < T/K < 300	298 K	300 < T/K < 323
$Sr_3Fe_{1.8}Co_{0.2}O_4Cl_2$	D1b, ILL	D1a, ILL	D2b, ILL
	λ = 2.52 Å	λ = 1.91 Å	λ = 1.59 Å
$Sr_3Fe_{1.4}Co_{0.6}O_4Cl_2$	D1b, ILL	D1a, ILL	
	λ = 2.52 Å	λ = 1.91 Å	
$Sr_3Fe_{1.2}Co_{0.8}O_4Cl_2$	D2b, ILL	D2b, ILL	
	λ = 1.59 Å	λ = 1.59 Å	
$Sr_3FeCoO_4Cl_2$	POLARIS, ISIS	POLARIS, ISIS	
	time of flight	time of flight	

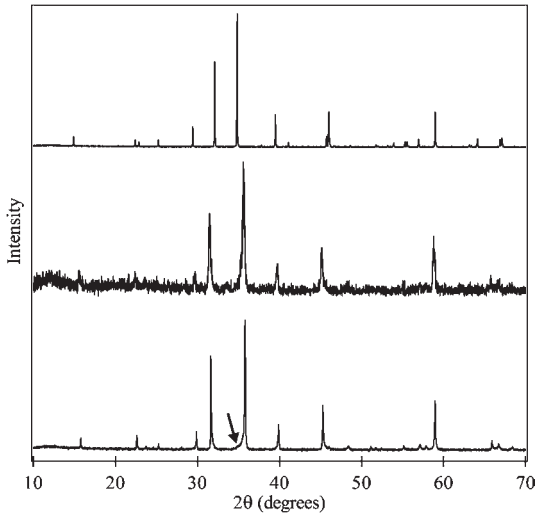

Figure 2. X-ray powder diffraction data collected from $Sr_3Fe_{1.8}Co_{0.2}O_5Cl_2$ (top), $Sr_3Fe_{1.8}Co_{0.2}O_4Cl_2$ prior to methanol wash (middle), and $Sr_3Fe_{1.8}Co_{0.2}O_4Cl_2$ after the methanol washing procedure (bottom). The arrow marks additional scattering due to the presence of $Sr_3Fe_{1.8}Co_{0.2}O_5Cl_2$.

at temperatures above 350 °C result in the decomposition of the $Sr_3Fe_{2-x}Co_xO_5Cl_2$ ($0.2 \leq x \leq 1$) substrate phases to form a complex mixture of binary metal oxides, chlorides, and elemental iron and cobalt. In the temperature range 300 < T/°C < 350 reactions resulted in the formation of body-centered tetragonal phases with lattice parameters similar to that of $Sr_3Fe_2O_4Cl_2$,[10] indicating that topotactic reduction reactions of the $Sr_3Fe_{2-x}Co_xO_5Cl_2$ ($0.2 \leq x \leq 1$) substrate phases had occurred.

Examination of X-ray powder diffraction data collected from samples before and after the methanol washing procedure (Figure 2) revealed a number of additional weak diffraction reflections in the latter data sets. These additional features are consistent with the presence of small amounts of oxidized $Sr_3Fe_{2-x}Co_xO_5Cl_2$ phases formed by mild oxidation during the washing procedure. The quantity of these oxidized phases could be minimized by the use of dry solvents and rigorously anaerobic conditions; however, with the exception of the $x = 1$ sample, their presence could not be completely eliminated. This high level of air sensitivity exhibited by $Sr_3Fe_{2-x}Co_xO_4Cl_2$ phases is consistent with the pyrophoric behavior of $Sr_3Fe_2O_4Cl_2$.[10]

Structural Characterization. Neutron powder diffraction data collected from the reduced $Sr_3Fe_{2-x}Co_xO_4Cl_2$ (x = 0.2, 0.6, 0.8, 1) samples could be readily indexed on the basis of body-centered tetragonal cells, with lattice parameters similar to those of $Sr_3Fe_2O_4Cl_2$. Structural models based on the refined structure of $Sr_3Fe_2O_4Cl_2$ were therefore constructed for the $Sr_3Fe_{2-x}Co_xO_4Cl_2$ phases and refined against these neutron powder diffraction data sets. As noted above the samples contained small quantities of $Sr_3Fe_{2-x}Co_xO_5Cl_2$ impurities; therefore, structural models based on $Sr_3Fe_{2-x}Co_xO_5Cl_2$ phases were added to the structural refinements to account for these diffraction features. Further additional diffraction features were observed in the room-temperature data collected from the $x = 0.2$ sample, which were consistent with the presence of long-range magnetic order, as observed previously for $Sr_3Fe_2O_4Cl_2$.[10] A magnetically ordered model was therefore added to the refinement performed against this data set, as described more fully below.

The structural refinements against all 4 room-temperature data sets converged readily to give good statistical fits to the data. To confirm the $Sr_3Fe_{2-x}Co_xO_4Cl_2$ composition of the bulk phases, the fractional occupancies of the oxygen and chlorine sites were refined and were observed to remain at fully occupancy, within error. In addition an extra oxide ion site was added at ($^1/_2$, $^1/_2$, 0) to model partial oxidation of the bulk phases. This site refined to zero occupancy for all samples, demonstrating that the mild oxidation observed during the methanol wash resulted in a mixture of $Sr_3Fe_{2-x}Co_xO_4Cl_2$ and $Sr_3Fe_{2-x}Co_xO_5Cl_2$ not some partially oxidized $Sr_3Fe_{2-x}Co_xO_{5-y}Cl_2$ phase. Full details of the structures refined for the $Sr_3Fe_{2-x}Co_xO_4Cl_2$ phases are given in Table 2 with selected bond lengths in Table 3. Observed, calculated and difference plots from the refinement of $Sr_3FeCoO_4Cl_2$ against neutron powder diffraction data are shown in Figure 3, with analogous plots from the room-temperature structural refinements of $Sr_3Fe_{2-x}Co_xO_4Cl_2$ (x = 0.2, 0.6, 0.8) given in the Supporting Information.

Magnetic Characterization. Variable temperature neutron powder diffraction data were collected from the $Sr_3Fe_{2-x}Co_xO_4Cl_2$ (x = 0.2, 0.6, 0.8, 1) samples, as described in Table 1, to characterize the long-range magnetic order in these phases. As reported previously, $Sr_3Fe_2O_4Cl_2$ adopts an antiferromagnetically ordered state below $T_N \sim 378$ K.[10] Examination of the variable temperature neutron powder diffraction data collected from $Sr_3Fe_{1.8}Co_{0.2}O_4Cl_2$ and $Sr_3Fe_{1.4}Co_{0.6}O_4Cl_2$ revealed diffraction features consistent with the $a' = \sqrt{2} \times a$, $b' = \sqrt{2} \times b$, $c' = c$ magnetic cell refined for $Sr_3Fe_2O_4Cl_2$; therefore, magnetic models analogous to that refined for $Sr_3Fe_2O_4Cl_2$ were refined against these data sets. Complete descriptions of these refinements are given in the Supporting Information.

Figure 4 shows a plot of the ordered magnetic moment refined for the $Sr_3Fe_{2-x}Co_xO_4Cl_2$ (x = 0, 0.2, and 0.6) phases as a function of temperature. Fits of these data to an $I = A(1 - (T/T_N))^{\beta}$ power law yielded values of β = 0.494, 0.495, and 0.394; T_N = 378 K, 340 K, and 300 K for the x = 0, 0.2, and 0.6 samples, respectively. There was no indication of magnetic order in either the x = 0.8 or x = 1 sample down to the lowest temperature measured (5 K).

Magnetic susceptibility data collected from $Sr_3FeCoO_4Cl_2$ using the "ferromagnetic subtraction" method described above, are shown in Figure 5. These data can be fitted to the Curie−Weiss law ($\chi = C/(T - \theta)$) in the temperature range $35 \leq T/K \leq 300$, to yield values of C = 0.778(4) cm^3 K mol^{-1} and $\theta = -9.7(3)$ K. It should be noted that this value of the Curie constant is significantly lower than would be expected for a simple

dx.doi.org/10.1021/ic200832n |Inorg. Chem. 2011, 50, 7250–7256

Table 2. Structural Parameters Refined for $Sr_3Fe_{2-x}Co_xO_4Cl_2$ Phases against Room-Temperature Neutron Powder Diffraction Data[a]

	$Sr_3Fe_{2-x}Co_xO_4Cl_2$				
	$x = 0$	$x = 0.2$	$x = 0.6$	$x = 0.8$	$x = 1$
a (Å)	4.0095(1)	4.0160(1)	4.0178(1)	4.0162(1)	4.0145(1)
c(Å)	22.6365(5)	22.6275(9)	22.552(1)	22.595(1)	22.4795(7)
Sr(1) U_{iso} (Å^2)	0.0054(2)	0.0072(18)	0.0136(21)	0.0104(15)	0.0038(4)
Sr(2) z	0.1524(1)	0.1526(1)	0.1526(2)	0.1528(2)	0.15309(7)
Sr(2) U_{iso} (Å^2)	0.0087(1)	0.0093(13)	0.0082(15)	0.0141(12)	0.0066(3)
Fe/Co z	0.4263(1)	0.4250(1)	0.4258(2)	0.4263(2)	0.42676(9)
Fe/Co U_{iso} (Å^2)	0.0048(1)	0.0061(7)	0.0032(8)	0.0023(2)	0.0021(2)
O z	0.4214(1)	0.4215(1)	0.4218(2)	0.4218(1)	0.42152(6)
O U_{iso} (Å^2)	0.0128(4)	0.0167(8)	0.0141(8)	0.0135(6)	0.0110(2)
Cl z	0.2950(1)	0.2948(1)	0.2954(1)	0.2956(1)	0.29492(6)
Cl U_{iso} (Å^2)	0.0135(3)	0.0121(7)	0.0122(8)	0.0134(6)	0.0129(2)
weight percent $Sr_3Fe_{2-x}Co_xO_5Cl_2$	0	15%	17%	13%	0
χ^2	4.6	1.88	1.529	2.318	1.284
diffractometer	D2B	D1A	D1A	D2B	POLARIS

[a] Sr(1) is located at (0,0,0); Sr(2) at (0,0,z); Fe/Co at (0,0,z); O at ($^1/_2$,0,z); Cl at (0,0,z). Data for the $x = 0$ sample are taken from reference 10 for comparison.

Table 3. Selected Bond Lengths Extracted from the Refinements of $Sr_3Fe_{2-x}Co_xO_4Cl_2$ Phases[a]

$Sr_3Fe_{2-x}Co_xO_4Cl_2$	Fe−O (Å)	Fe−Cl (Å)	Sr(1)−O (Å)	Sr(2)−O (Å)	Sr(2)−Cl (Å)	Sr(2)−Cl (Å)
$x = 0$	2.008(1)	2.972(3)	2.680(2)	2.610(2)	3.075(1)	3.228(3)
$x = 0.2$	2.010(1)	2.946(3)	2.681(1)	2.616(2)	3.079(1)	3.218(3)
$x = 0.6$	2.011(1)	2.941(5)	2.673(3)	2.617(4)	3.074(2)	3.220(5)
$x = 0.8$	2.011(1)	2.940(5)	2.670(1)	2.617(3)	3.068(2)	3.212(5)
$x = 1$	2.011(1)	2.964(2)	2.672(1)	2.616(1)	3.070(1)	3.188(2)

[a] Data for the $x = 0$ sample are taken from reference 10 for comparison.

paramagnet ($C_{expected} = 4.87$ cm^3 K mol^{-1} assuming high-spin, $S = 2$ Fe^{2+} and high-spin, $S = {}^3/_2$ Co^{2+}). Below this temperature range there is a maximum in the magnetic susceptibility at $T \sim 25$ K, indicative of a magnetic transition. This feature is associated with a sharp increase in the saturated ferromagnetic moment of the sample, from an essentially temperature independent value of ~1000 emu mol^{-1} in the range $35 < T/K < 300$ (attributable to the presence of elemental iron and cobalt), to 2500 emu mol^{-1} at 5 K. Magnetization-field isotherms collected from $Sr_3FeCoO_4Cl_2$ (Figure 6) reflect this change in saturated ferromagnetic moment. Furthermore close inspection of the field-cooled isotherm collected at 5 K (inset to Figure 6) reveal the magnetization-field loop is displaced to higher magnetization, consistent with spin-glass type behavior. This suggests that the anomalies observed in the magnetic data at $T \sim 25$ K are associated with a transition to a spin-glass like behavior.

Magnetic susceptibility data collected from the remaining $Sr_3Fe_{2-x}Co_xO_4Cl_2$ ($x = 0.2, 0.6, 0.8$) samples exhibit the same general features as the data collected from $Sr_3FeCoO_4Cl_2$ (Supporting Information). Table 4 lists the Curie constants and Weiss temperatures extracted from these data in the temperature range $35 \leq T/K \leq 300$.

DISCUSSION

The reaction of phases in the composition range $Sr_3Fe_{2-x}Co_xO_5Cl_2$ ($0 \leq x \leq 1$) with LiH results in the deintercalation of oxide ions from these materials to yield products of composition $Sr_3Fe_{2-x}Co_xO_4Cl_2$ which are isostructural to the previously reported phase $Sr_3Fe_2O_4Cl_2$.[10] The observation that the partial substitution of iron with cobalt does not change the structural selectivity of the reaction between $Sr_3Fe_2O_5Cl_2$ and LiH is in agreement with the strong lattice energy driven preference for the removal of the bridging oxide ion from $Sr_3Fe_2O_5Cl_2$, described previously.[10] Furthermore the formation of square planar Co(II) centers in the resulting $Sr_3Fe_{2-x}Co_xO_4Cl_2$ phases appears to present no energetic barrier to the reaction. This is consistent with the relative prevalence of square planar $Co^{II}O_4$ centers in thermodynamically stable extended solids (in $Sr_2CoO_2Cl_2$ and $Ba_2CoO_2Cu_2S_2$ for example)[16,17] compared to the paucity of the analogous $Fe^{II}O_4$ centers. The limited influence of cobalt on the formation of $Sr_3Fe_{2-x}Co_xO_4Cl_2$ phases is in strong contrast to that of the $SrFeO_{3-\delta}$−$SrFeO_2$ system, in which replacing more than 30% of the iron centers with cobalt or manganese changes the structure of the reduced product.[9] This difference strongly suggest that different factors are directing the anion vacancy order in the $Sr_3Fe_2O_5Cl_2$−$Sr_3Fe_2O_4Cl_2$ and $SrFeO_{3-\delta}$−$SrFeO_2$ systems, the A-cation lattice in the former case and some electronic factor in the latter.

The influence of cobalt substitution on the structural parameters of $Sr_3Fe_2O_4Cl_2$ is minimal. The a-lattice parameter and in-plane Co−O bonds appear unchanged within error across the $Sr_3Fe_{2-x}Co_xO_4Cl_2$ ($0 \leq x \leq 1$) series (Table 3). The c-lattice

dx.doi.org/10.1021/ic200832n |Inorg. Chem. 2011, 50, 7250–7256

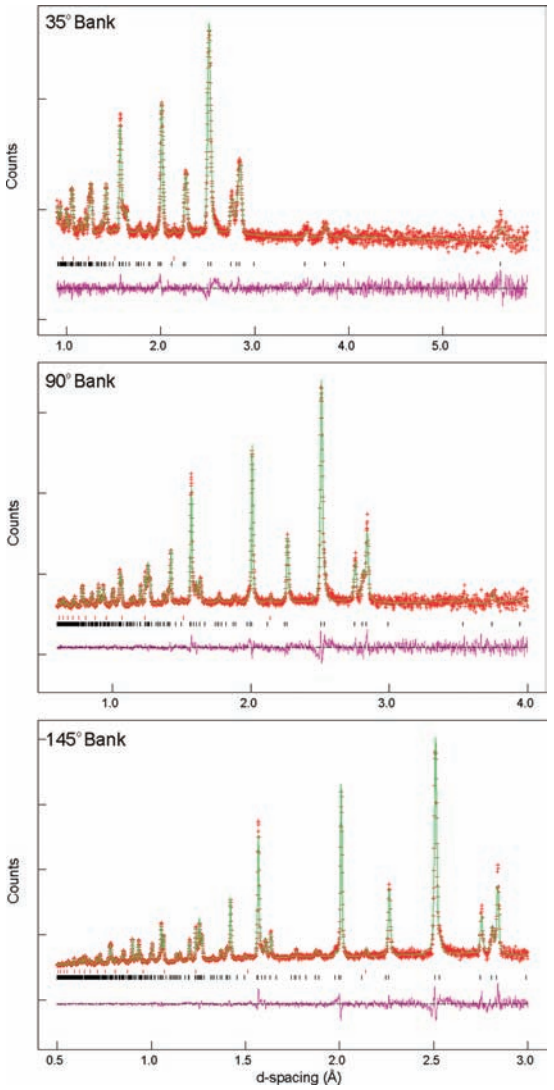

Figure 3. Observed, calculated, and difference plots from the structural refinement of $Sr_3FeCoO_4Cl_2$ against room-temperature neutron powder diffraction data collected using the POLARIS diffractometer. The lower set of tick marks indicate peak positions for $Sr_3FeCoO_4Cl_2$, upper tick marks indicate peak positions for the vanadium sample holder.

parameter contracts by ~0.7% across the compositional range associated with a general contraction of the structure in this direction. The slight scatter in the data in Tables 2 and 3 as a function of cobalt concentration is attributable to the systematic errors introduced by collecting the neutron powder diffraction data utilized in the structural refinements, using three different diffractometers (Table 1).

The influence of cobalt substitution on the magnetic behavior of $Sr_3Fe_2O_4Cl_2$ is more striking. As shown in Figure 4, substitution of iron with cobalt leads to as steady depression of the antiferromagnetic ordering temperature of $Sr_3Fe_{2-x}Co_xO_4Cl_2$ phases followed by a complete suppression of long-range magnetic order for samples with $x \geq 0.8$. The mechanism by which cobalt substitution suppresses long-range magnetic order can be elucidated by examining the paramagnetic susceptibility data collected from $Sr_3Fe_{2-x}Co_xO_4Cl_2$ samples and considering the magnetic coupling interactions present in these phases. As shown in Table 4, the Curie constants extracted from the susceptibility

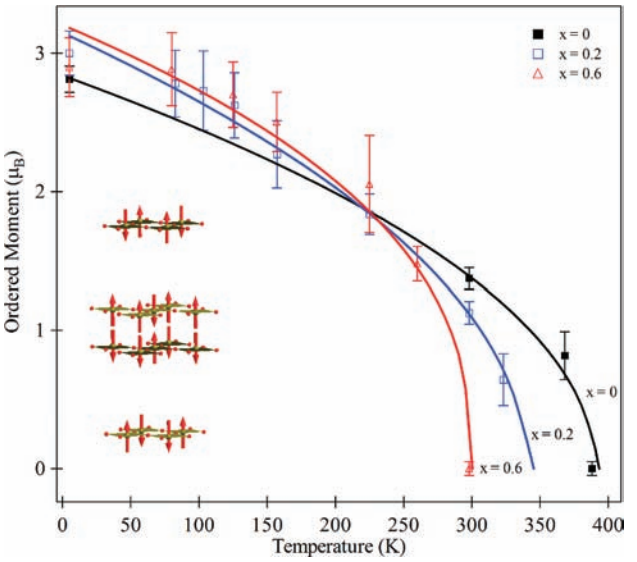

Figure 4. Plot of the refined ordered magnetic moment as a function of temperature for $Sr_3Fe_{2-x}Co_xO_4Cl_2$ (x = 0, 0.2, 0.6) phases. Inset shows the antiferromagnetically ordered structure of the $Sr_3Fe_{2-x}Co_xO_4Cl_2$ (x = 0, 0.2, 0.6) phases. Data for the x = 0 sample are taken from ref 10.

data collected from $Sr_3Fe_{2-x}Co_xO_4Cl_2$ samples are significantly smaller than would be expected for simple paramagnetic behavior, representing between 6 and 25% of the value predicted for spin-only behavior. These low values are entirely expected for $Sr_3Fe_{1.8}Co_{0.2}O_4Cl_2$ and $Sr_3Fe_{1.4}Co_{0.6}O_4Cl_2$ as these phases exhibit long-range antiferromagnetic order at temperatures below 340 K and 300 K, respectively (Figure 4). In this instance the observed paramagnetic susceptibility is attributable to uncoupled spins at grain boundaries and other defect or surface sites. The weak paramagnetic responses of the remaining $Sr_3Fe_{2-x}Co_xO_4Cl_2$ ($x \geq 0.8$) phases are more surprising, as they imply that even in the absence of long-range magnetic order there are still strong antiferromagnetic correlations between spins. When combined with the displaced magnetization-field loops at low temperature (Figure 6), this suggests that the substitution of iron with cobalt adds additional magnetic interactions into the $Sr_3Fe_{2-x}Co_xO_4Cl_2$ system which compete with and frustrate long-range antiferromagnetic order, ultimately leading to glassy magnetic behavior.

As noted previously the local electronic configuration of Fe(II) centers in $Sr_3Fe_2O_4Cl_2$ is $(d_{z^2})^2(d_{xz}, d_{yz})^2(d_{xy})^1(d_{x^2-y^2})^1$ as shown in Figure 7a.[10,18] The Goodenough−Kanamouri rules[19] predict strong antiferromagnetic superexchange within the FeO_2 planes of $Sr_3Fe_2O_4Cl_2$ through 180°, σ-type Fe $(d_{x^2-y^2})^1$−O $(2p)$−Fe $(d_{x^2-y^2})^1$ coupling (Figure 7c). In addition we would expect antiferromagnetic direct σ-exchange coupling between the two full Fe $(d_{z^2})^2$ orbitals, expectations which are consistent with the high-temperature antiferromagnetic order observed in the all-iron phase. The electronic configuration of square-planar $Co^{II}O_4$ centers is predicted to be $(d_{z^2})^2(d_{xz}, d_{yz})^3(d_{xy})^1(d_{x^2-y^2})^1$ (Figure 7b) by analogy to other structurally related phases containing square-planar Co(II) centers.[17] Thus the partial substitution of Fe(II) with Co(II) in $Sr_3Fe_{2-x}Co_xO_4Cl_2$ phases retains local electronic configurations on all transition metal centers suitable for strong antiferromagnetic σ-exchange coupling (i.e., a full $(d_{z^2})^2$ orbital and a half-full $(d_{x^2-y^2})^1$ orbital). However, the presence of an additional electron in the degenerate d_{xz}, d_{yz} pair of orbitals of Co(II) centers

dx.doi.org/10.1021/ic200832n |Inorg. Chem. 2011, 50, 7250–7256

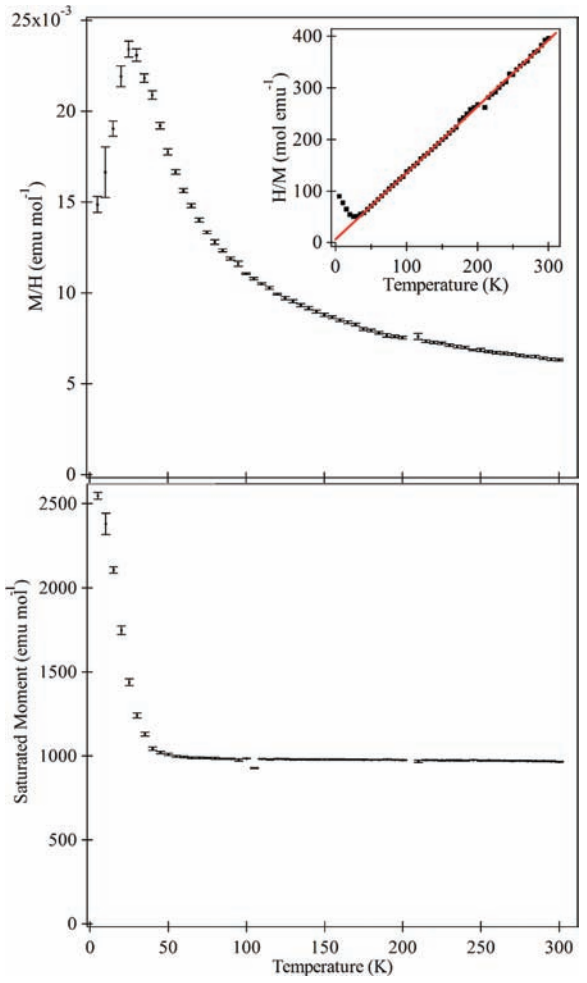

Figure 5. Magnetization data collected from $Sr_3FeCoO_4Cl_2$ using the "ferromagnetic subtraction" method. Upper panel shows the paramagnetic susceptibility as a function of temperature. Inset shows a fit to the Curie−Weiss law in the temperature range $35 \leq T/K \leq 300$. Lower panel shows the saturated ferromagnetic moment as a function of temperature.

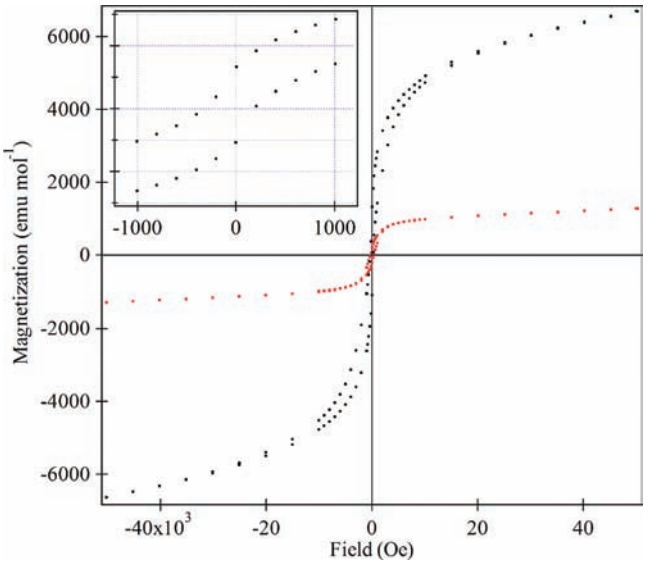

Figure 6. Magnetization-field isotherms collected at 300 K (red) and 5 K (black) from $Sr_3FeCoO_4Cl_2$. Inset shows an expanded region of the 5 K isotherm emphasizing that the data are displaced to higher magnetizations.

Table 4. Parameters Extracted from Fits to the Magnetic Susceptibility Data Collected from $Sr_3Fe_{2-x}Co_xO_4Cl_2$ Samples in the Temperature Range $35 \leq T/K \leq 300$[a]

$Sr_3Fe_{2-x}Co_xO_4Cl_2$	C_{obs} (cm^3 K mol^{-1})	C_{exp} (cm^3 K mol^{-1})	θ (K)
$x = 0.2$	0.357(3)	5.775	−2.4(6)
$x = 0.6$	1.213(5)	5.325	−2.3(3)
$x = 0.8$	0.732(9)	5.10	−5.6(4)
$x = 1$	0.788(4)	4.875	−9.7(3)

[a] Expected Curie constants are calculated using the spin-only moments of high-spin Fe^{2+} ($S = 2$) and high-spin Co^{2+} ($S = {}^3/_2$).

introduces the possibility of π-type Co $(d_{xz}/d_{yz})^2$−O $(2p_z)$−Fe $(d_{xz}/d_{yz})^1$ (Figure 7d) superexchange coupling which would be expected to be ferromagnetic. This ferromagnetic interaction will compete with the antiferromagnetically coupled σ-exchange network and other π-type couplings such as Co$(d_{xz}/d_{yz})^1$−O$(2p_z)$−Fe$(d_{xz}/d_{yz})^1$ (Figure 7c) which are also antiferromagnetic. We propose that it is this competition between the ferromagnetic π-superexchange coupling (attributable to the extra valence electron associated with Co(II) compared with Fe(II)) and the underlying network of antiferromagnetic interactions which leads to the suppression of long-range magnetic order on cobalt substitution, and ultimately glassy behavior in $Sr_3Fe_{2-x}Co_xO_4Cl_2$ ($x \geq 0.8$) phases.

Recently Kageyama et al. have reported the successful preparation of cobalt substituted $SrFeO_2$,[9] the three-dimensional structural analogue of $Sr_3Fe_2O_4Cl_2$. In this study it is observed that in the limited substitution range that can be prepared ($0 \leq x \leq 0.3$) cobalt doping has only a minor effect on the magnetic behavior of $SrFe_{1-x}Co_xO_2$ phases. All compositions exhibit long-range antiferromagnetic order at room-temperature with observed ordered moments which are almost independent of cobalt concentration. Room-temperature Mössbauer spectra collected from these phases allow the authors to estimate that a 30% cobalt substitution level reduces the antiferromagnetic ordering temperature by "no more than 50 K".[9] While it is hard to accurately quantify the influence of the cobalt concentration on the magnetic behavior of $SrFe_{1-x}Co_xO_2$ from the data presented, it does appear that the substitution of cobalt for iron in $SrFeO_2$ has a weaker disruptive influence on the antiferromagnetic order exhibited by the undoped phase, than the analogous substitution in the $Sr_3Fe_{2-x}Co_xO_4Cl_2$ system (at 30% substitution $\Delta T_N = 80$ K for $Sr_3Fe_{2-x}Co_xO_4Cl_2$; $\Delta T_N < 50$ K for $SrFe_{1-x}Co_xO_2$). The greater robustness to disruption by substitution of the underlying antiferromagnetically ordered network of $SrFeO_2$ is attributable to the more three-dimensional nature of the $SrFeO_2$ structure compared to the more two-dimensional $Sr_3Fe_2O_4Cl_2$. This is also consistent with the observed antiferromagnetic ordering temperatures of 473 and 378 K for $SrFeO_2$ and $Sr_3Fe_2O_4Cl_2$, respectively. We would therefore predict that cation substitutions at the iron coordination sites in the one-dimensional phase $Sr_3Fe_2O_5$[6] would have an even greater effect on the magnetic behavior of this material than those observed for either $SrFeO_2$ or $Sr_3Fe_2O_4Cl_2$.

In conclusion, we have prepared phases of composition $Sr_3Fe_{2-x}Co_xO_4Cl_2$ ($0 \leq x \leq 1$) which contain sheets of apex-linked square-planar $(Fe/Co)O_4$ centers. Addition of cobalt

dx.doi.org/10.1021/ic200832n |*Inorg. Chem.* 2011, 50, 7250–7256

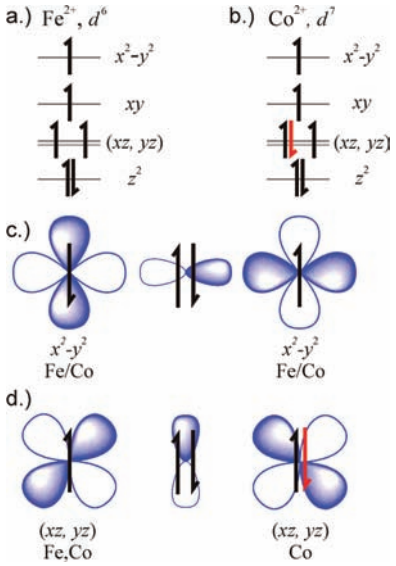

Figure 7. (a) Local electronic state of square-planar Fe^{2+} centers. (b) The local electronic state of square-planar Co^{2+} centers. (c) A representation of the orbitals involved in antiferromagnetic σ-type Fe/Co $(d_{x^2-y^2})^1$—O $(2p)$—Fe/Co $(d_{x^2-y^2})^1$ superexchange. (d) A representation of the orbitals involved in ferromagnetic π-type Co $(d_{xz}/d_{yz})^2$—O $(2p_z)$—Fe $(d_{xz}/d_{yz})^1$ superexchange.

suppresses the antiferromagnetic order of the $Sr_3Fe_2O_4Cl_2$ host phase leading to spin-glass behavior in $Sr_3Fe_{2-x}Co_xO_4Cl_2$ phases with $x \geq 0.8$.

■ ASSOCIATED CONTENT

Supporting Information. Description of the magnetic measurement procedure for samples containing elemental cobalt impurities. The refined lattice parameters of $Sr_3Fe_{2-x}Co_xO_5Cl_2$ $(0 \leq x \leq 1)$ phases. Observed, calculated, and difference plots from the room-temperature structural refinements of $Sr_3Fe_{2-x}Co_xO_4Cl_2$ (x = 0.2, 0.6, 0.8) and the structural and magnetic refinements of $Sr_3Fe_{2-x}Co_xO_4Cl_2$ (x = 0.2, 0.6) against data collected at 5 K. Magnetization data collected from $Sr_3Fe_{2-x}Co_xO_4Cl_2$ (x = 0.2, 0.6, 0.8). This material is available free of charge via the Internet at http://pubs.acs.org.

■ AUTHOR INFORMATION

Corresponding Author

*Phone: +44 1865 272623. Fax: +44 1865 272690. E-mail: michael.hayward@chem.ox.ac.uk.

■ ACKNOWLEDGMENT

We thank R. Smith and E. Suard for assistance in collecting the neutron diffraction data. Experiments at the ISIS pulsed neutron facility were supported by a beam time allocation from the Science and Technology Facilities Council. E.D. thanks the EPSRC for a studentship.

■ REFERENCES

(1) Hayward, M. A.; Green, M. A.; Rosseinsky, M. J.; Sloan, J. *J. Am. Chem. Soc.* **1999**, *121*, 8843.
(2) Crespin, M.; Landron, C.; Odier, P.; Bassat, J. M.; Mouron, P.; Choisnet, J. *J. Solid State Chem.* **1992**, *100*, 281.
(3) Siegrist, T.; Zahurak, S. M.; Murphy, D. W.; Roth, R. S. *Nature* **1988**, *334*, 231.
(4) Weller, M. T.; Lines, D. R. *J. Solid State Chem.* **1089**, *82*, 21.
(5) Tsujimoto, Y.; Tassel, C.; Hayashi, N.; Watanabe, T.; Kageyama, H.; Yoshimura, K.; Takano, M.; Ceretti, M.; Ritter, C.; Paulus, W. *Nature* **2007**, *450*, 1062.
(6) Hiroshi, K.; Takashi, W.; Yoshihiro, T.; Atsushi, K.; Yuji, S.; Kazuyoshi, K.; Kazuyoshi, Y.; Naoaki, H.; Shigetoshi, M.; Mikio, T.; Monica, C.; Werner, P.; Clemens, R.; Gilles, A. *Angew. Chem.* **2008**, *47*, 5740.
(7) O'Malley, M.; Lockett, M. A.; Hayward, M. A. *J. Solid State Chem.* **2007**, *180*, 2851.
(8) Seddon, J.; Suard, E.; Hayward, M. A. *J. Am. Chem. Soc.* **2010**, *132*, 2802.
(9) Seinberg, L.; Yamamoto, T.; Tassel, C.; Kobayashi, Y.; Hayashi, N.; Kitada, A.; Sumida, Y.; Watanabe, T.; Nishi, M.; Ohoyama, K.; Yoshimura, K.; Takano, M.; Paulus, W.; Kageyama, H. *Inorg. Chem.* **2011**, *50* (9), 3988–3995.
(10) Dixon, E.; Hayward, M. A. *Inorg. Chem.* **2010**, *49*, 9649.
(11) Knee, C. S.; Field, M. A. L.; Weller, M. T. *Solid State Sci.* **2004**, *6*, 443.
(12) Grenier, J. C.; Ghodbane, S.; Demazeau, G.; Pouchard, M.; Hagenmuller, P. *Mater. Res. Bull.* **1979**, *14*, 831.
(13) Adkin, J. J.; Hayward, M. A. *Inorg. Chem.* **2008**, *47*, 10959.
(14) Larson, A. C.; Von Dreele, R. B. General Structure Analysis System (GSAS), Los Alamos National Laboratory Report LAUR 86-748; Los Alamos National Laboratory: Los Alamos, NM, 2000.
(15) Hayward, M. A.; Rosseinsky, M. J. *Chem. Mater.* **2000**, *12*, 2182.
(16) Knee, C. S.; Weller, M. T. *Phys. Rev. B* **2004**, *70*, 144406.
(17) Smura, C. F.; Parker, D. R.; Zbiri, M.; Johnson, M. R.; Gal, Z. A.; Clarke, S. J. *J. Am. Chem. Soc.* **2011**, *133*, 2691.
(18) Xiang, H. J.; Wei, S.-H.; Whangbo, M. H. *Phys. Rev. Lett.* **2008**, *100*, 167207.
(19) Goodenough, J. B. *Magnetism and the Chemical Bond*; Wiley: New York, 1963.